J. Fluid Mech. (1997), *vol.* 343, *pp.* 351–373. Printed in the United Kingdom

Wave propagation in porous media containing a dilute gas–liquid mixture: theory and experiments

By D. M. J. SMEULDERS[1] AND M. E. H. VAN DONGEN[2]

[1]Delft University of Technology, PO Box 5028, 2600 GA Delft, The Netherlands

[2]Eindhoven University of Technology, PO Box 513, 5600 MB Eindhoven, The Netherlands

(Received 13 May 1996 and in revised form 11 March 1997)

The influence of a small amount of gas within the saturating liquid of a porous medium on acoustic wave propagation is investigated. It is assumed that the gas volumes are spherical, homogeneously distributed, and that they are within a very narrow range of bubble sizes. It is shown that the compressibility of the saturating fluid is determined by viscous, thermal, and a newly introduced Biot-type damping of the oscillating gas bubbles, with mean gas bubble size and concentration as important parameters. Using a super-saturation technique, a homogeneous gas–liquid mixture within a porous test column is obtained. Gas bubble size and concentration are measured by means of compressibility experiments. Wave reflection and propagation experiments carried out in a vertical shock tube show pore pressure oscillations, which can be explained by incorporating a dynamic gas bubble behaviour in the linear Biot theory for plane wave propagation.

1. Introduction

The acoustic properties of liquid-saturated porous media are very sensitive to the presence of a small amount of gas in the pores. In seismic engineering practice, this may affect the interpretation of the reflected waves from the subsurface geological strata. In petrophysics, acoustic borehole tools are basically used to measure reservoir porosities. These measurements also are influenced by low concentrations of gaseous inclusions. An extended literature survey was given by Anderson & Hampton (1980*a*, *b*). More recently, Biot's two-phase theory was modified to allow for the presence of a gas phase. Garg & Nayfeh (1986) and Berryman, Thigpen & Chin (1988) present rather general models, applicable to a wide range of gas volume fractions. The effect of a small number of oscillating gas bubbles on the propagation and damping of compressional waves in porous media was also described by Bedford & Stern (1983). Experimental data in this field are given by Dontsov, Kuznetsov & Nakoryakov (1987) and van der Grinten *et al.* (1988), who used a shock tube technique to induce compressional waves in a porous cylinder. Sniekers *et al.* (1989) and Smeulders, De la Rosette & van Dongen (1992*a*) also presented wave measurements on dilute gas–liquid mixtures in porous media and made preliminary comparisons with linear wave theory, but they did not discuss the thermal damping nor did they take into account the compressibility effects of the fluid–solid system.

In this paper, the damped oscillations of an isolated gas bubble in the saturating liquid of a porous sample will be studied. Viscous and thermal damping mechanisms

are identified and quantified. A Biot-type damping mechanism is introduced. Following van Wijngaarden (1972), who studied wave propagation in bubbly liquids, we assume that the results obtained for the isolated bubble will also hold in the case of a mixture of liquid and gas bubbles. Secondly, a homogeneous mixture of liquid and gas bubbles is prepared within the pores of a cylindrical sample. Gas bubble size and concentration are independently measured by means of compressibility experiments. Thirdly, wave experiments are carried out in a shock tube and pore pressures are measured and compared with linear Biot theory for plane wave propagation, which is modified to account for the behaviour of the gas bubbles.

2. General relations

We start with the conservation laws of mass and momentum for two interacting media of a porous system, namely solid material indicated by the subscript s and pore fluid, indicated by the subscript f. The gas bubbles will not be treated as a separate medium, but they will be considered as part of the pore fluid. This means that (Bear & Bachmat 1990, pp. 78, 79)

$$\frac{\partial}{\partial t}(\phi_m \rho_m) + \frac{\partial}{\partial x_j}(\phi_m \rho_m v_{mj}) = 0, \tag{2.1}$$

$$\frac{\partial}{\partial t}(\phi_m \rho_m v_{mi}) + \frac{\partial}{\partial x_j}(\phi_m \rho_m v_{mj} v_{mi}) = -\frac{\partial}{\partial x_j}(\phi_m p_{mji}) + f_{mi}, \tag{2.2}$$

where summation over repeated index j is assumed. The subscript m is either s or f, ϕ_m is the volume fraction of component m, p_m the pressure or compressive stress, ρ_m the density, v_m the velocity and f_m represents the interaction force. It is assumed that the solid temperature does not change. $\phi_f = 1 - \phi_s$ is also known as the porosity. The compressive stress acting in a cross-section of porous material consists of two contributions: $p_{sji} = p_f \delta_{ij} + \sigma_{ji}/\phi_s$. The so-called intergranular stress σ_{ij} is related to the change in porosity: $\phi_f = \phi_f(\sigma_{ij})$. The density of the solid material is considered constant. For the fluid we may write $p_{fji} = p_f \delta_{ij}$. The interaction term f_{mi} is specified in its linear form:

$$f_{fi} = -f_{si} = p_f \frac{\partial}{\partial x_i}(\phi_f) + b_0 w_i + \phi_f \rho_f (\alpha_\infty - 1)\frac{\partial w_i}{\partial t}, \tag{2.3}$$

where we have introduced the velocity difference vector $\boldsymbol{w} = \boldsymbol{v}_s - \boldsymbol{v}_f$. The second term on the right-hand side of (2.3) represents the steady-state friction. The friction factor b_0 is related to the steady-state permeability k_0 by $b_0 = \eta \phi_f^2 / k_0$, with η the viscosity. The last term on the right-hand side of (2.3) represents the added mass effect, with α_∞ the added mass parameter or tortuosity (Biot 1956*a*).

The continuity relations (2.1) may be linearized and combined. For our experiments it is reasonable to assume that the solid grains are incompressible ($d\rho_s = 0$). We then find

$$\frac{\partial \phi_f}{\partial t} = (1 - \phi_f)\nabla \cdot \boldsymbol{v}_s, \tag{2.4}$$

$$-\frac{\phi_f}{\rho_f}\frac{\partial \rho_f}{\partial t} = \phi_s \nabla \cdot \boldsymbol{v}_s + \phi_f \nabla \cdot \boldsymbol{v}_f. \tag{2.5}$$

3. Plane wave propagation

We will now consider the propagation of plane compressional waves within a system of Cartesian coordinates. Velocities in the (X, Y)-plane are neglected and the field variables depend on z and t only. The linearized momentum equations for the solid and for the fluid can be derived from (2.2) and (2.3) and were given by Biot (1956*a*):

$$\phi_s\rho_s\frac{\partial v_s}{\partial t} = -\frac{\partial \sigma_{zz}}{\partial z} - \phi_s\frac{\partial p_f}{\partial z} - b_0 w - \phi_f\rho_f(\alpha_\infty - 1)\frac{\partial}{\partial t}(v_s - v_f), \tag{3.1}$$

$$\phi_f\rho_f\frac{\partial v_f}{\partial t} = -\phi_f\frac{\partial p_f}{\partial z} + b_0 w + \phi_f\rho_f(\alpha_\infty - 1)\frac{\partial}{\partial t}(v_s - v_f), \tag{3.2}$$

where v_s and v_f the velocity components in the z-direction. Using the time derivative of Hooke's law, the intergranular stress can be related to the solid velocity:

$$-\frac{\partial \sigma_{zz}}{\partial t} = K_p\frac{\partial v_s}{\partial z}, \tag{3.3}$$

where K_p is the constrained modulus of the matrix, related to the matrix bulk and shear moduli K_b and G by $K_p = K_b + \frac{4}{3}G$. In (3.3), it is assumed that the grains are incompressible (Verruijt 1982). The fluid density and the fluid pressure are related via the bulk modulus of the fluid $K_f = \rho_f(\partial\rho_f/\partial p_f)^{-1}$. Introduction of K_f in (2.5) yields the so-called storage equation, which forms a basic relation in consolidation problems (Verruijt 1982):

$$-\frac{\phi_f}{K_f}\frac{\partial p_f}{\partial t} = \phi_s\frac{\partial v_s}{\partial z} + \phi_f\frac{\partial v_f}{\partial z}. \tag{3.4}$$

We proceed with the substitution of (3.3) and (3.4) into the momentum equations (3.1) and (3.2). Assuming a harmonic variation for all field variables, i.e. $v_m = \hat{v}_m(r)\exp(\mathrm{i}\omega t)$, etc., we find

$$-\phi_s\rho_s\omega^2\hat{v}_s = P\hat{D}_s + Q\hat{D}_f - (\hat{v}_s - \hat{v}_f)[\mathrm{i}\omega b - (\alpha_\infty - 1)\phi_f\rho_f\omega^2], \tag{3.5}$$

$$-\phi_f\rho_f\omega^2\hat{v}_f = Q\hat{D}_s + R\hat{D}_f + (\hat{v}_s - \hat{v}_f)[\mathrm{i}\omega b - (\alpha_\infty - 1)\phi_f\rho_f\omega^2], \tag{3.6}$$

where we introduced the Biot constants $P = K_p + K_f\phi_s^2/\phi_f$, $Q = \phi_s K_f$ and $R = \phi_f K_f$. Obviously, it is not *a priori* necessary to assume that the solid grains are incompressible, as we did in (2.4), (2.5), (3.3), and (3.4). Detailed expressions for the Biot constants that allow for compressible grains were discussed by Geertsma & Smit (1961), Stoll (1974) and Allard (1993).

Furthermore, we have defined a spatial derivative operator:

$$\hat{D}_m = \frac{\partial^2}{\partial z^2}\hat{v}_m, \tag{3.7}$$

where the subscript m is either s or f. Note that the previously used steady-state parameter b_0 has been replaced by $b(\omega)$, describing the more realistic frequency-dependent Darcy interaction force between the fluid and the solid. At low frequencies, $b(\omega)$ will show a Stokes-flow behaviour, whereas at higher frequencies, when the viscous skin depth $\delta = (2\eta/\omega\rho_f)^{1/2}$ decreases, inertial effects will become dominant. This behaviour can also be described by a frequency-dependent tortuosity $\alpha(\omega)$ (Johnson & Plona 1982). It was shown that $\alpha(\omega) = \alpha_\infty - [\mathrm{i}b(\omega)/\omega\phi\rho_f]$. A thorough theoretical and experimental description of these phenomena was given by Lévy (1979), Auriault (1980), Auriault, Borne & Chambon (1985), Johnson, Koplik & Dashen (1987), Smeulders, Eggels & van Dongen (1992*b*) and Smeulders *et al.*

(1994). The solution of (3.5) and (3.6) is given by $\hat{v}_m = A_m \exp(-\mathrm{i}kz)$, where k is the wavenumber and A_m is an arbitrary constant. Following van der Grinten, van Dongen & van der Kogel (1985, 1987), two equations for A_s and A_f are obtained from which the dispersion relation is found:

$$d_2\zeta^2 + d_1\zeta + d_0 = 0, \tag{3.8}$$

where $\zeta = k^2/\omega^2$ and

$$\left.\begin{aligned} d_2 &= PR - Q^2, \\ d_1 &= -(P\rho_{22} + R\rho_{11} - 2Q\rho_{12}) + \mathrm{i}b/\omega(P + R + 2Q), \\ d_0 &= \rho_{11}\rho_{22} - \rho_{12}^2 - \mathrm{i}b\rho/\omega. \end{aligned}\right\} \tag{3.9}$$

The density terms are defined in agreement with Biot (1956*a*):

$$\rho_{12} = -(\alpha_\infty - 1)\phi_f\rho_f, \quad \rho_{11} = \phi_s\rho_s - \rho_{12}, \quad \rho_{22} = \phi_f\rho_f - \rho_{12}, \quad \rho = \rho_{11} + \rho_{22} + 2\rho_{12}.$$

The dispersion relation (3.8) has two complex roots ζ_1 and ζ_2 and there are therefore two damped compression waves, also called P-waves (Biot 1956*a*). For the velocities of the solid and the fluid, we may now write

$$\hat{v}_s = A_{s1}\mathrm{e}^{-\mathrm{i}k_1 z} + A_{s2}\mathrm{e}^{-\mathrm{i}k_2 z}, \tag{3.10}$$

$$\hat{v}_f = \beta_1 A_{s1}\mathrm{e}^{-\mathrm{i}k_1 z} + \beta_2 A_{s2}\mathrm{e}^{-\mathrm{i}k_2 z}, \tag{3.11}$$

where for both wave modes $j = 1, 2$ the fluid–solid amplitude ratios $\beta_j = A_{fj}/A_{sj}$ follow from either (3.5) or (3.6). The wavenumbers k_j are fully determined by (3.8) as a function of the properties of the porous material and its saturating fluid.

If the saturating fluid consists of a liquid–gas mixture, the contributions of the liquid and the gas are taken into account in the fluid bulk modulus (Wood 1955, p. 361):

$$\frac{1}{K_f} = \frac{s}{K_l} + \frac{1-s}{K_g}, \tag{3.12}$$

where we have denoted the liquid fraction in the pores by s (saturation) and the gas fraction in the pores by $1 - s$. K_l is the bulk modulus of the pure liquid and K_g is an effective bulk modulus of the gas phase, which relates the averaged gas volume V_g to a change in liquid pressure $p_{f\infty}$ far away from the gas volume: $K_g = -V_g(\partial V_g/\partial p_{f\infty})^{-1}$. This approach is similar to the treatment of wave propagation in bubbly liquids by, among others, van Wijngaarden (1970, 1972). If the behaviour of the gas volume is considered isothermal and quasi-stationary, $K_g = p_g$, where p_g is the pressure within the gas volume. In the next sections, the damped oscillations of an isolated gas bubble within the saturating liquid in the pores are studied, and a relation between the liquid pressure far away from the bubble and the gas bubble volume is derived. This relation is written as a complex-valued frequency-dependent effective bulk modulus of the gas bubble. Next, following van Wijngaarden (1972), we will assume that the same effective bulk modulus is valid for a homogeneous distribution of gas bubbles within a very narrow range of bubble sizes.

4. Biot damping

The purpose of §§4 to 6 is to determine the damping mechanisms of oscillating bubbles in a porous system. Obviously, this problem is closely related to the study of small-amplitude acoustic wave propagation in bubbly liquids. Foldy (1945) showed

that for small gas fractions the velocity and the damping of the waves can be determined to the order $(1-s)$ by describing the interaction of a single bubble with the wave. Sangani (1991) determined the higher-order corrections to Foldy's equations by considering the bubble oscillations not in the pure liquid but in a medium that has a much higher compressibility due to the presence of the other surrounding bubbles. Therefore, the main difference between the Foldy and the Sangani models is in the estimate of the acoustic radiation damping, as was also discussed in a paper by Sangani & Sureshkumar (1993). The Sangani theory significantly improved the agreement between experimental data and model computations for bubble frequencies lower than and close to the bubble resonant frequency. In a porous medium however, a complicating aspect is that the bubble is not surrounded by just one single compressible medium, but by both the compressible pore fluid and the compressible matrix. This means that the corresponding damping is described by the bubble emitting two spherical Biot waves. The energy distribution over both waves is determined by the boundary conditions at the bubble interface. Therefore, in a porous system the radiation damping is replaced by a so-called Biot damping, which consists of fluid and matrix compressibility effects (true radiation damping), and Darcy interaction effects between the pore fluid and the solid matrix. In the previous Section, we showed that this Darcy interaction can effectively be described by the parameter $b(\omega)$. As a matter of fact, it turns out that for frequencies lower than or close to the bubble resonant frequency, the Darcy part of the Biot damping strongly dominates the true radiation damping. Following Foldy, we will therefore not apply higher-order corrections to the compressibility of the pore fluid.

It is clear that the oscillations of gas fractions in a porous medium depend on the shape and structure of those gas fractions. From visualization experiments in an optically transparant porous material, we have learned that the gas fractions that occur commonly occupy several pores and have a ramified shape, e.g. like alveoli in the human lungs. Yet, the general character of the gas fractions is still spherical, with part of the internal gas volume being occupied by skeletal material. Therefore, in the forthcoming sections, the analysis is based upon this assumption of sphericity. We will consider an isolated gas bubble and let the origin of coordinates be at the bubble centre, which is at rest. The radius of the bubble at any time t is $a(t)$ and r is the radius to any point in the solid or in the liquid. The gas volume $V_g = \frac{4}{3}\phi_f a^3$. Within a system of spherical coordinates (r, ϕ, θ), the field variables describing wave motions with polar symmetry depend on r and t only. The single velocity components v_s and v_f are in the radial direction. From (2.2) and (2.3), the linearized radial momentum equations for the solid and the fluid become (see also Achenbach 1973, p. 128)

$$\mathrm{i}\omega\phi_s\rho_s\hat{v}_s = -\frac{\partial\hat{\sigma}_{rr}}{\partial r} - \frac{2(\hat{\sigma}_{rr}-\hat{\sigma}_{\phi\phi})}{r} - \phi_s\frac{\partial\hat{p}_f}{\partial r} - b\hat{w} - \mathrm{i}\omega\phi_f\rho_f(\alpha_\infty - 1)\hat{w}, \tag{4.1}$$

$$\mathrm{i}\omega\phi_f\rho_f\hat{v}_f = -\phi_f\frac{\partial\hat{p}_f}{\partial r} + b\hat{w} + \mathrm{i}\omega\phi_f\rho_f(\alpha_\infty - 1)\hat{w}, \tag{4.2}$$

where $\sigma_{\phi\phi} = \sigma_{\theta\theta}$ is the normal stress in any direction perpendicular to r. Hooke's law for both stress components may be written (Achenbach 1973, p. 77)

$$-\mathrm{i}\omega\hat{\sigma}_{rr} = (K_b - \tfrac{2}{3}G)\nabla\cdot\hat{\boldsymbol{v}}_s + 2G\frac{\partial\hat{v}_s}{\partial r}, \tag{4.3}$$

$$-\mathrm{i}\omega\hat{\sigma}_{\phi\phi} = (K_b - \tfrac{2}{3}G)\nabla\cdot\hat{\boldsymbol{v}}_s + 2G\frac{\hat{v}_s}{r}, \tag{4.4}$$

where K_b is the bulk modulus and G the shear modulus of the matrix structure.

Repeating the same procedures as in the case of one-dimensional wave propagation, we end up with relations corresponding to (3.5) and (3.6). In this case, however, the spatial derivative operator $\hat{D}_m$ takes a different form. We find that it is convenient to express the radial velocities in terms of potential functions $\hat{v}_m = \partial\hat{\Phi}_m/\partial r$, which yields

$$\hat{D}_m = \frac{\partial^2\hat{v}_m}{\partial r^2} + \frac{2}{r}\frac{\partial\hat{v}_m}{\partial r} - \frac{2\hat{v}_m}{r^2} = \frac{\partial}{\partial r}\left[\frac{1}{r}\frac{\partial^2}{\partial r^2}(r\hat{\Phi}_m)\right]. \tag{4.5}$$

The solution of (3.5) and (3.6) is now given by

$$r\hat{\Phi}_s = A_{s1}\mathrm{e}^{-\mathrm{i}k_1 r} + A_{s2}\mathrm{e}^{-\mathrm{i}k_2 r}, \tag{4.6}$$

$$r\hat{\Phi}_f = \beta_1 A_{s1}\mathrm{e}^{-\mathrm{i}k_1 r} + \beta_2 A_{s2}\mathrm{e}^{-\mathrm{i}k_2 r}, \tag{4.7}$$

where k_1 and k_2 are the wavenumbers of both modes and β_1 and β_2 are the fluid–solid amplitude ratios defined in the previous Section. In order to obtain the equation of motion for the bubble, (4.2) is integrated over the fluid from $r = a$ to infinity:

$$\phi_f\rho_f\omega^2\hat{\Phi}_{fa} = -\mathrm{i}\omega\phi_f(\hat{p}_{f\infty} - \hat{p}_{fa}) + \omega^2\rho'_{12}(\hat{\Phi}_{fa} - \hat{\Phi}_{sa}), \tag{4.8}$$

where $\rho'_{12} = \rho_{12} + \mathrm{i}b/\omega$. Substitution of (4.6) and (4.7) into (4.8) yields

$$\rho_f\omega^2\left[b_1A'_1 + b_2A'_2\right] = -\mathrm{i}\omega\phi_f(\hat{p}_{f\infty} - \hat{p}_{fa}), \tag{4.9}$$

where for both wave modes $j = 1, 2$ we have introduced

$$b_j = \phi_f\beta_j - (\beta_j - 1)\frac{\rho'_{12}}{\rho_f}, \quad A'_j = \frac{A_{fj}}{a}\mathrm{e}^{-\mathrm{i}k_j a}.$$

For the matrix structure within the gas bubble surface ($r < a$), we may neglect the interaction effects between the matrix and the gas. The gas bulk modulus is negligible compared with the bulk modulus of the matrix. In this case, (3.5) becomes

$$-\phi_s\rho_s\omega^2\hat{v}_s = K_p\hat{D}_s\,. \tag{4.10}$$

Assuming that the Helmholtz number $ka \ll 1$, where $k^2 = \omega^2\phi_s\rho_s/K_p$, it follows that the matrix within the bubble surface may be regarded as acoustically compact: $\hat{D}_s = 0$. Using (4.5) yields that the solid velocities within the bubble surface are directly proportional to r. This means that

$$\left[\frac{\partial\hat{v}_s}{\partial r}\right]_a = \left[\frac{\hat{v}_s}{r}\right]_a. \tag{4.11}$$

From (2.4), it can also be found that the porosity within the bubble surface must be uniform, i.e. not a function of r. This implies that the mass conservation law (2.5) may be integrated over the volume V_g/ϕ_f within the bubble surface to find an equation which directly relates a change in gas bubble volume to the fluid and matrix velocities at the bubble surface ($r = a$):

$$\mathrm{i}\omega\hat{V}_g = 4\pi a^2\left(\phi_s\hat{v}_{sa} + \phi_f\hat{v}_{fa}\right). \tag{4.12}$$

Substitution of (4.6) and (4.7) into (4.11) and (4.12) yields another two equations for the previously defined parameters A'_j:

$$a_1A'_1 + a_2A'_2 = 0, \tag{4.13}$$

$$c_1A'_1 + c_2A'_2 = -\mathrm{i}\omega\frac{\hat{V}_g}{4\pi a}, \tag{4.14}$$

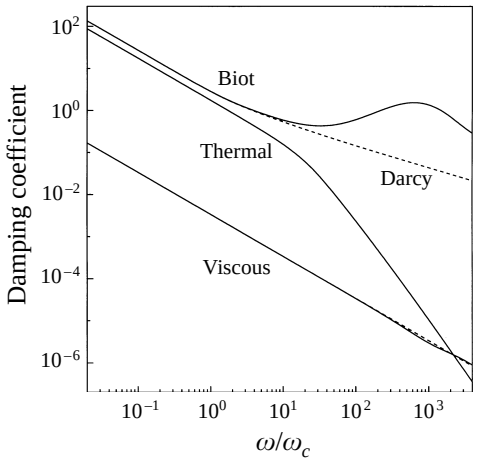

FIGURE 1. Damping coefficients of freely oscillating gas bubbles in a saturated porous medium as a function of the reduced frequency. Bubble radius: 1 mm. Dashed lines refer to an incompressible pore fluid and an incompressible porous matrix. ω_c is defined in (4.16).

where

$$a_j = k_j^2 \left(1 - 3\,\frac{1 + \mathrm{i}k_j a}{k_j^2 a^2}\right),$$

$$c_j = (1 + \mathrm{i}k_j a)\left(1 - \phi_f + \phi_f \beta_j\right).$$

From (4.9), (4.13) and (4.14), a relation between the driving pressure $\hat{p}_{f\infty}$ and the change in the gas bubble volume may be found by eliminating the coefficients A'_j:

$$\omega^2 \rho_f \left(\frac{a_1 b_2 - a_2 b_1}{a_1 c_2 - a_2 c_1}\right) \frac{\hat{V}_g}{4\pi\phi_f a} = \hat{p}_{f\infty} - \hat{p}_{fa}. \tag{4.15}$$

This is a modified version of the well-known Rayleigh–Plesset equation, which was originally derived to describe the oscillating behaviour of gas bubbles in a surrounding fluid (Plesset 1949; van Wijngaarden 1970). Note that the term $\hat{V}_g/(4\pi\phi_f a)$ equals $a\hat{a}$. The imaginary part of the term between brackets in (4.15) accounts for the Biot damping consisting of Darcy damping and compressibility effects. The fluid surrounding the bubble provides the inertia for this system, as can be seen on the left-hand side of (4.15). As discussed previously, the Darcy friction originates from the relative velocity of the fluid with respect to the solid matrix as a result of the gas bubble oscillations. Obviously this term is not present in the original Rayleigh–Plesset equation. A plot of the newly introduced Biot damping as a function of the reduced frequency is given in figure 1 for a bubble radius $a = 1$ mm. The other parameter values are given in table 1. The characteristic frequency is defined in agreement with our earlier work (Smeulders *et al.* 1992*b*):

$$\omega_c = \eta\phi_f / k_0 \alpha_\infty \rho_f. \tag{4.16}$$

For a gas bubble surrounded by an incompressible fluid and an incompressible solid matrix, only the pure Darcy damping is left. In this case (4.15) becomes

$$\omega^2 \rho_f \left(1 - \frac{\rho'_{12}}{\phi_f \rho_f}\right) \frac{\hat{V}_g}{4\pi\phi_f a} = \hat{p}_{f\infty} - \hat{p}_{fa}. \tag{4.17}$$

Porosity	ϕ_f	0.29
Viscosity	η (Pa s^{-1})	0.001
Matrix bulk modulus	K_p (10^9 Pa)	10.2
Fluid bulk modulus	K_f (10^9 Pa)	2.2
Tortuosity	α_∞	2.7
Grain density	ρ_s (kg m^{-3})	2650.0
Fluid density	ρ_f (kg m^{-3})	1000.0
Permeability	k_0 (10^{-12} m^2)	90.91

TABLE 1. Parameter values

The imaginary part of the term between brackets now represents the pure Darcy damping coefficient which is also drawn in figure 1. It becomes clear that the true radiation damping, represented by the difference between the Biot and the Darcy damping, is negligible for low frequencies, and only becomes important for higher frequencies. In figure 1, the viscous damping and the thermal damping are also drawn. These mechanisms will be discussed in the next sections.

5. Viscous damping at the bubble surface

In order to eliminate the liquid pressure p_{fa} in (4.15) and (4.17), we will now consider the pressure difference over the bubble surface and assume that it is balanced by the radial viscous stress in the fluid at the bubble surface (Bird, Stewart & Lightfoot 1960, p. 90):

$$p_{fa} - p_g = \eta \left(2\frac{\partial v_f}{\partial r} - \tfrac{2}{3}\nabla \cdot \boldsymbol{v}_f \right)_a \tag{5.1}$$

where p_g is the gas bubble pressure. For our experimental conditions the effects of surface tension can be neglected. Furthermore, the gas bubble pressure is assumed to be uniform throughout the bubble, which implies that the inertia and the viscosity of the gas are negligible. The same approach was used by Dontsov *et al.* (1987), who also ignored surface tension effects. Assuming a harmonic dependence for the relevant parameters, using (4.6) and (4.7) for the velocities, and eliminating A_1' and A_2' from (4.13) and (4.14), we find from (5.1):

$$\hat{p}_{fa} - \hat{p}_g = \tfrac{4}{3}\mathrm{i}\omega\eta \frac{a_1 a_2(\beta_2 - \beta_1)}{a_1 c_2 - a_2 c_1} \frac{\hat{V}_g}{4\pi a}. \tag{5.2}$$

Substitution of (5.2) into the Rayleigh–Plesset equation (4.15) yields

$$\omega^2 \rho_f \left[\frac{a_1 b_2 - a_2 b_1}{a_1 c_2 - a_2 c_1} + \frac{4}{3}\frac{\mathrm{i}\eta\phi_f}{\omega\rho_f} \frac{a_1 a_2(\beta_2 - \beta_1)}{a_1 c_2 - a_2 c_1} \right] \frac{\hat{V}_g}{4\pi\phi_f a} = \hat{p}_{f\infty} - \hat{p}_g. \tag{5.3}$$

The imaginary part of the second term between the brackets in (5.3) is the dimensionless viscous damping coefficient. For a bubble radius $a = 1$ mm, the viscous term is plotted in figure 1. The other parameters are given in table 1. Over the entire frequency range the viscous damping appears to be much less important than the Biot damping. In the case of an incompressible fluid–solid system, the above procedures can be repeated, and (5.3) transforms into

$$\omega^2 \rho_f \left(1 - \frac{\rho_{12}'}{\phi_f \rho_f} - \frac{4\mathrm{i}\eta}{a^2 \omega \rho_f} \right) \frac{\hat{V}_g}{4\pi\phi_f a} = \hat{p}_{f\infty} - \hat{p}_g. \tag{5.4}$$

The viscous damping term in this relation is exactly as defined by van Wijngaarden (1972), and is also plotted in figure 1. It is interesting to notice that over the entire frequency range the viscous damping is virtually unaffected by the compressibility of the fluid–solid system. A comparison between the viscous and Biot damping is determined by the ratio $4k_0/a^2\phi$, which is of the order 10^{-3} for our experiments.

6. Thermal damping

The thermal damping of an oscillating gas bubble submerged in an infinitely extended fluid has been investigated by, amoung others, Pfriem (1940), Spitzer (1943), Devin (1959), and Prosperetti (1984, 1991). These theories will now be modified and applied to the case of an oscillating gas bubble in a fluid-saturated porous medium. As we stated previously, a gas bubble with radius a in a fluid-saturated porous medium will commonly occupy several pores: $a > R$, where R is a characteristic pore radius. As before we define a spherical coordinate system originating at the centre of the bubble. The bubble, which is in an alternating pressure field $p_{f\infty}$, can only be in equilibrium with this oscillating pressure by pulsating itself. We will now consider a cycle of vibration of the bubble. As the bubble is compressed its temperature T rises; when the rise of the temperature is appreciable, heat conduction becomes important and the bubble tends to cool off even before the expansion has started. We assume that the heat conduction will take place from the gas phase to the porous matrix and we will neglect any heat flow from the bubble to the surrounding pore fluid. When maximum compression is reached the temperature will already be decreasing as heat flows from the bubble into the surrounding grains. It is obvious that in this case maximum temperature will be reached somewhat before maximum compression is established. Therefore the temperature of the bubble at a given volume will be somewhat greater during the compression part of a cycle than during the expansion part. Since there is a direct relation between volume and pressure of the gas bubble, at a given volume the pressure exerted on the bubble during the compression will be greater than the corresponding pressure during the expansion. Hence more energy is required to compress the bubble than is regained in the subsequent expansion. The work done by the bubble during one cycle of its vibration is negative and represents a net flow of heat into the surrounding grains. For a compressible perfect gas, the linearized energy equation becomes (Devin 1959)

$$\frac{\partial(rT)}{\partial t} = a_g \frac{\partial^2(rT)}{\partial r^2} + \frac{r}{\rho_g c_p}\frac{\partial p_g}{\partial t}, \tag{6.1}$$

where a_g is the thermal diffusivity of the gas phase and c_p the specific heat at constant pressure. We have neglected the viscous dissipation within the bubble and we have considered the heat flow as a result of conduction alone. This is because convection is unimportant, as the time factor for establishment of this process is considerably larger than the time taken for a half-cycle vibration of the bubble. Assuming an $\exp(\mathrm{i}\omega t)$ dependence for all relevant quantities and satisfying the boundary conditions that the linearized temperature variation $\hat{T}$ must be finite at the centre of the bubble and zero at the gas–grain interface, (6.1) may be solved:

$$r\hat{T} = \frac{R\hat{p}_g}{c_p\rho_g}\left[\frac{r}{R} - \frac{\sinh(\psi r)}{\sinh(\psi R)}\right], \tag{6.2}$$

where $\psi = (1+\mathrm{i})(\omega/2a_g)^{1/2}$. This relation is basically the same as the one found by Devin (1959), who necessarily introduced a instead of R as the relevant length scale.

The heat flow rate $\hat{Q}_R$ (i.e. unit energy per unit time) from the part of the bubble volume occupying one single pore to the surrounding grains may now be calculated. It is proportional to the temperature gradient at the gas–grain interface: $\hat{Q}_R = 4\pi R^2 \lambda_g [\partial \hat{T}/\partial r]_R$, where λ_g is the thermal conductivity of the gas phase. The total heat flow rate $\hat{Q}$ away from the bubble may subsequently be obtained by taking into account the total gas bubble volume: $\hat{Q} = \phi_f (a/R)^3 \hat{Q}_R$. From (6.2), we may then write

$$\hat{Q} = 3V_g a_g \hat{p}_g \psi^2 \left[\frac{\coth(\psi R)}{(\psi R)} - \frac{1}{(\psi R)^2} \right], \tag{6.3}$$

where we have written $V_g = \frac{4}{3}\pi\phi_f a^3$. We find that the heat conduction process is governed by the parameter (ψR) and thus by the ratio R/δ_T, where $\delta_T = (2a_g/\omega)^{1/2}$ is the thermal depth of penetration.

It is also possible to calculate the internal energy $\hat{E}_R$ of the part of the bubble volume occupying one single pore. We will consider this volume as the sum of all concentric shells with radius r and thickness dr. For each shell the temperature is known according to relation (6.2) and consequently also the internal energy $\mathrm{d}\hat{E}_R = \rho_g c_v \hat{T} 4\pi r^2 \mathrm{d}r$, where c_v is the specific heat at constant volume. Subsequent substitution of (6.2) and integration from zero to R yields $\hat{E}_R$. For the total internal energy $\hat{E}$ of the gas bubble we may consequently write

$$\hat{E} = \phi_f \left(\frac{a}{R} \right)^3 \hat{E}_R = V_g \frac{\hat{p}_g}{\gamma} \left[1 + \frac{3}{(\psi R)^2} - \frac{3}{(\psi R)} \coth(\psi R) \right], \tag{6.4}$$

where $\gamma = c_p/c_v$. Apparently, the internal energy is also determined by the ratio R/δ_T. The time derivative of the internal energy must obey the first law of thermodynamics, which is written in the form

$$\mathrm{i}\omega \hat{E} = -\hat{Q} - \mathrm{i}\omega p_g \hat{V}_g, \tag{6.5}$$

where a harmonic variation has been substituted for all relevant quantities. Please note that the minus-sign in front of $\hat{Q}$ is a consequence of our definition of the direction of the heat flow, which has been chosen positive when flowing from the gas bubble towards the surrounding grains. From (6.5) it becomes obvious that a relation between the change in volume and the change in pressure of the gas bubble may be found after substitution of (6.3) and (6.4):

$$\frac{\hat{p}_g}{p_g} = -n \frac{\hat{V}_g}{V_g}, \tag{6.6}$$

where we have introduced a complex-valued polytropic exponent n:

$$n = \gamma \left\{ 1 + 3(\gamma - 1) \left[\frac{\coth(\psi R)}{(\psi R)} - \frac{1}{(2\psi R)^2} \right] \right\}^{-1}. \tag{6.7}$$

This relation may be compared with the ones proposed by Devin (1959) and Prosperetti (1984, 1991) for oscillating bubbles in a liquid. It is found that for porous media the pore radius R is used instead of the bubble radius a. We assume that R is to a good approximation equal to the viscous length scale $\Lambda = (8\alpha_\infty k_0/\phi_f)^{1/2}$, introduced by Johnson *et al.* (1987). A plot of the real and imaginary parts of n is presented in figure 2. For small values of R/δ_T an isothermal behaviour is observed: $n \to 1.0$. In the limit of high R/δ_T values the process will behave isentropically: $n \to \gamma = 1.4$. In between there is a transition zone with a non-zero imaginary part of n, which causes

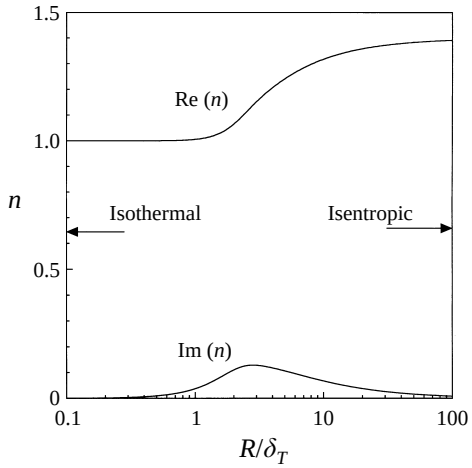

FIGURE 2. Real and imaginary parts of the polytropic exponent n as a function of the pore radius over the thermal penetration depth.

a phase difference between the pressure and the volume variations of the gas bubble. This imaginary part of n is therefore responsible for the thermal damping. This can be seen by substituting $\hat{p}_g$ from (6.6) into (5.3). The dimensionless thermal damping coefficient may then be written

$$\delta_{th} = \frac{3p_g \,\mathrm{Im}(n)}{\rho_f \omega^2 a^2}. \tag{6.8}$$

For a gas pressure $p_g = 10^5$ Pa and a bubble radius $a = 1$ mm, the thermal damping is plotted in figure 1. In the lower frequency range, the thermal damping is of the same order of magnitude as the Biot damping, but for higher frequencies it becomes relatively less important. Champoux & Allard (1991) and Henry *et al.* (1995) argue that a more general expression for the polytropic exponent can be given:

$$n = \gamma \left\{ \gamma - (\gamma - 1) \left[1 - \frac{4\mathrm{i}}{(\Lambda'/\delta_T)^2} \left(1 + \tfrac{1}{8}\mathrm{i}(\Lambda'/\delta_T)^2 \right)^{1/2} \right]^{-1} \right\}^{-1}, \tag{6.9}$$

where Λ' is a thermal length scale, defined as a pore volume-to-surface ratio:

$$2/\Lambda' = \int \mathrm{d}S \Big/ \int \mathrm{d}V. \tag{6.10}$$

Both expressions for the polytropic exponent (6.7) and (6.9) are characterized by a low-frequency limit and by an asymptotic behaviour for high frequencies. It can be shown that these characteristics are identical in both expressions, if a thermal length scale $\Lambda' = 2R/3$ is introduced in (6.7), which is in agreement with the definition of Λ' in (6.10).

7. Dynamic compressibility

Taking into account all the damping mechanisms that we considered in the previous sections, it is now possible to calculate the effective bulk modulus of the isolated gas

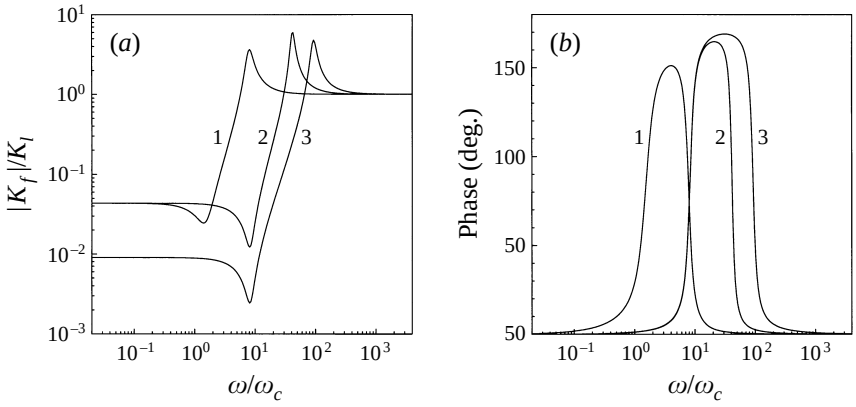

FIGURE 3. Absolute (*a*) and phase values (*b*) of the fluid bulk modulus as a function of the reduced frequency for different bubble radii a and gas volume fractions $(1-s)$. 1: $a = 5$ mm and $(1-s) = 0.1\%$. 2: $a = 1$ mm and $(1-s) = 0.1\%$. 3: $a = 1$ mm and $(1-s) = 0.5\%$. ω_c is defined in (4.16).

bubble $K_g = -V_g(\partial V_g/\partial p_{f\infty})^{-1}$. Combination of (5.3) and (6.6) yields

$$K_g = \tfrac{1}{3}a^2\omega^2\rho_f\left[\frac{3np_g}{a^2\omega^2\rho_f} - \frac{a_1b_2 - a_2b_1}{a_1c_2 - a_2c_1} - \frac{4}{3}\frac{\mathrm{i}\eta\phi_f}{\omega\rho_f}\frac{a_1a_2(\beta_2-\beta_1)}{a_1c_2 - a_2c_1}\right]. \tag{7.1}$$

In the case of an incompressible fluid–solid system, we find that

$$K_g = \tfrac{1}{3}a^2\omega^2\rho_f\left(\frac{3np_g}{a^2\omega^2\rho_f} - 1 + \frac{\rho'_{12}}{\phi_f\rho_f} + \frac{4\mathrm{i}\eta}{a^2\omega\rho_f}\right). \tag{7.2}$$

This last relation for K_g was reported previously by Smeulders *et al.* (1992*a*) for isothermal behaviour of the gas bubbles, i.e. $n = 1$. If the viscous damping term is also ignored, we find an expression for the effective bulk modulus which was reported by Sniekers *et al.* (1989). Following van Wijngaarden (1972), we will now assume that (7.1) also holds for a saturating fluid containing a large number of homogeneously distributed bubbles within a very narrow range of bubble sizes. Combination of (3.12) and (7.1) then determines the bulk modulus of the fluid as a whole. Results are given in figures 3(*a*) and 3(*b*) for gas fractions of 0.1% and 0.5% and gas bubble radii of 1 and 5 mm. The bulk modulus of the liquid $K_l = 2.2$ GPa. For low frequencies, the gas bubbles vibrate isothermally and $K_g = p_g = 10^5$ Pa. As $K_g \ll K_l$, even small gas fractions substantially decrease the low-frequency bulk modulus of the fluid. For $(1-s) = 0.1\%$, we may compute the low-frequency ratio of the bulk moduli: $|K_f|/K_l = 4.35 \times 10^{-2}$ (see curves 1 and 2 in figure 3*a*), and for $(1-s) = 0.5\%$, we find that this ratio is 9.01×10^{-3} (curve 3). In the high-frequency limit, $K_g \to -\infty$ and therefore $K_f \to K_l/s$. This means that for small gas saturations the high-frequency compressibility is hardly affected by the gas in the pores, as is clearly visible in figure 3(*a*). The minimum absolute values of the bulk moduli are determined by the resonant frequency of the gas bubbles $\omega_r = (p_g/\alpha_\infty\rho_f a^2)^{1/2}$. The gas bubbles are vibrating in phase with the exerted fluid pressure which results in a highly compressible fluid. The minima are not determined by the gas saturation as can be seen from curves 2 and 3 in figure 3(*a*). The maximum values of the bulk moduli occur at the so-called anti-resonant frequencies of the gas bubbles. This means that an increase in fluid pressure causes the gas bubbles to expand. They are vibrating out of phase, which leads to a very incompressible pore fluid. This is neatly illustrated in the phase plot,

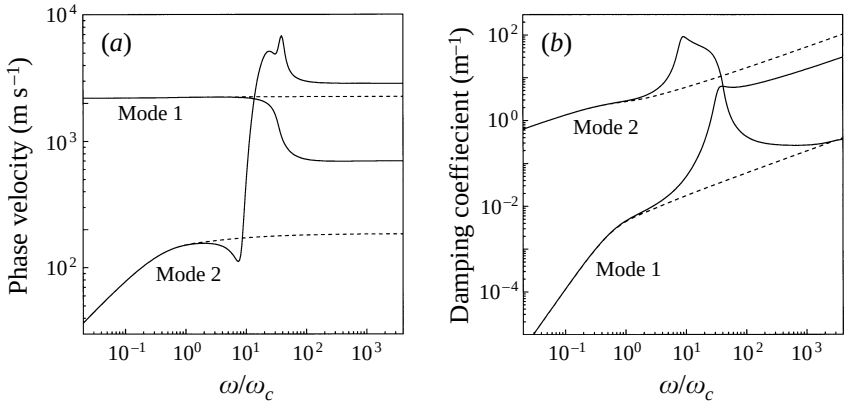

FIGURE 4. Phase velocities (*a*) and attenuation coefficients (*b*) of compression waves in a porous medium with water and equally sized gas bubbles as a function of the reduced frequency. Gas volume fraction: 0.1%. Gas bubble radius: 1 mm. The dashed lines refer to the quasi-stationary model. ω_c is defined in (4.16).

where values of over 150° are reached in the transition from in-phase to out-of-phase behaviour. From figure 3(*a*), it also becomes clear that the maxima are determined both by the gas bubble size and by the gas saturation.

Having determined $K_f(\omega)$ in this way, the dispersion relation (3.8) can now be solved. A comparison is made with a quasi-stationary model, in which the gas bubble oscillations are not taken into account: $K_f(\omega) = K_f(0)$. The results are shown in figures 4(*a*) and (*b*), where the phase velocities $\omega/\mathrm{Re}(k_j)$ and the damping coefficients $\mathrm{Im}(k_j)$ are plotted as a function of the reduced frequency. For the quasi-stationary model (dashed lines), our results are similar to the ones presented by Biot (1956*a*, *b*). Two wave modes are found, and mode 1 is faster and less damped for all frequencies. For the partially saturated case, dispersion calculations were previously presented by Smeulders *et al.* (1992*a*), but only Darcy and viscous damping were taken into account. Similar computations were also carried out by Bedford & Stern (1983), but they considered the thermal damping as the prevailing mechanism. We notice that a small amount of gas substantially influences phase velocities and damping coefficients. The velocity of the second wave mode reaches its maximum when the gas bubbles are vibrating out of phase, which results in a very incompressible fluid. The damping of the second wave reaches its maximum at the gas bubble resonant frequency, where the fluid is very compressible and the velocity of the second wave has a local minimum. The transition from in-phase to out-of-phase behaviour of the gas bubbles could be interpreted as a mode switch: the velocity of mode 1 becomes greater than of mode 2 and the damping of mode 1 becomes greater than of mode 2. But in fact this interchange of roles is a matter of academic interest only, because all resulting pressure computations are determined by a summation of both wave modes. Finally, in the high-frequency limit, the effects of the gas in the pores can be completely neglected, and the resulting velocities and damping coefficients are the same as in the fully saturated case.

8. Experimental set-up

The experimental set-up consists of a vertical shock tube with a length of about 8 m and an internal diameter of 77 mm. This set-up has been described by different

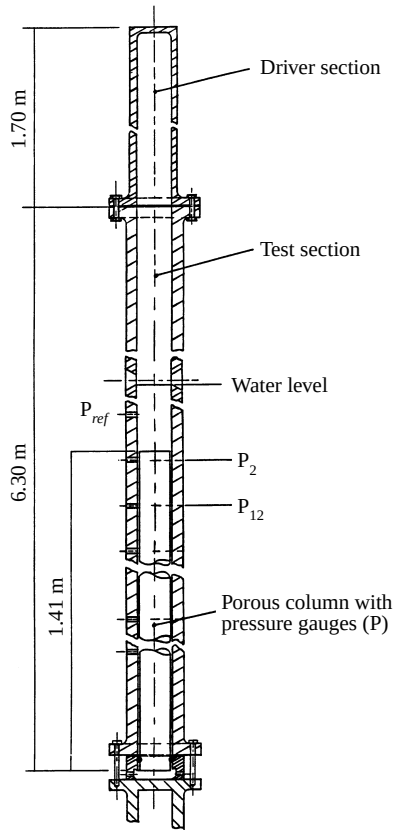

FIGURE 5. Experimental set-up for wave experiments in a porous medium. The test sample is placed in the test section of the shock tube.

authors like van der Grinten *et al.* (1985, 1987), Sniekers *et al.* (1989) and Smeulders *et al.* (1992*a*). A similar shock tube technique for the experimental investigation of wave propagation in porous media was also used by Dontsov *et al.* (1987). The set-up is drawn in figure 5. The shock tube sections are made out of steel and have a wall thickness of 24 mm. Below, in the test section, we have placed a cylindrical test sample with a length L_c of 1.41 m and a diameter d_c of 74 mm. For our experiments $L_c > \lambda/4$, where λ is a typical acoustic wavelength. The sample is a porous matrix, consisting of sand grains glued to each other by means of an epoxy resin. The diameter of an individual sand grain is approximately 0.5 mm. The properties of the test column are listed in tabel 1. Please note that these properties were all determined independently. The gap of 1.5 mm between the walls of the shock tube and the porous column is in order to prevent any shear interaction between the walls of the shock tube and the porous sample. The sidewall of the sample is covered with an epoxy coating (Sigma, Colturiet TCN), in order to prevent any lateral fluid flow through the sample wall. The sample is equipped with two miniature pore pressure transducers (Druck PDCR 81, without ceramic filters), located at 2 and 12 cm from the top of the sample. Finally, we have mounted a piezoelectric pressure gauge (Kistler 603B) in the shock tube wall 46 cm above the top of the porous column (see figure 5) to record the incident and reflected waves and to trigger the data recording system.

The preparation of the pore fluid, consisting of a water–air mixture, proceeds as

follows. First, the porous sample is fully water saturated. This is done by carefully evacuating the sample and filling the pores with carbon dioxide. Subsequently, the sample is filled with de-gassed water. The water level in the shock tube is indicated in figure 5. Carbon dioxide is far more soluble in water than air, thus causing a complete dissolution of any gas remnants. Next, in a separate vessel, an amount of water is saturated with air, at a constant pressure level, by blowing air bubbles into the vessel. The amount of air dissolving in the water is controlled by the vessel pressure, which is higher than the atmospheric pressure. By means of a rotary pump, this air-saturated water is flushed through the porous column until its entire pore volume has been refreshed about 50 times. Meanwhile, the porous column is held at the same pressure as within the vessel, and the blowing of air bubbles continues. Finally, the circulation is stopped, and the pressure is released. The pore fluid is now a super-saturated (200–300%) air solution. Gas molecules start to form gas bubble nuclei, which may take place at any microscopic roughness in the pore surface. This process is called heterogeneous nucleation. A description of this process and of the subsequent conditions for bubble growth is given by Ward *et al.* (1983). The spontaneous (homogeneous) formation of air bubbles does not occur. For this process a super-saturated air solution of 2000% is needed (van Stralen & Cole 1979).

The growth of the nuclei into fully fledged bubbles is a diffusion-dominated process, with gas bubble size and distribution as important parameters. These parameters are determined from a series of pore fluid compressibility measurements during the process of bubble growth. This measurement proceeds as follows. The pore fluid is subjected to a small pressure increase Δp during a time interval τ (typically of the order of several minutes), which is short enough to ensure that almost no gas from the bubble is dissolved in the surrounding liquid. From the corresponding change in liquid volume, the 'frozen' compressibility of the pore fluid is found, which is a direct measure for the gas fraction. The change in liquid volume is registered using a laser beam reflection from the water surface in the shock tube (van der Grinten *et al.* 1988). By repeating the 'frozen' compressibility measurements, the gradual change of the gas fraction $(1-s)$ towards a new equilibrium state can be measured and compared with diffusion theory (see the Appendix). Using a least-squares method, the best match for air bubble size and concentration to diffusion theory is obtained. In figure 6, an air bubble growth curve is plotted as a function of reduced time tD_e/a_e^2, where D_e is the effective diffusion constant of the liquid, and $2a_e$ is the average distance between gas bubbles. Each circle in the figure represents a 'frozen' compressibility experiment. When the gas bubbles have reached equilibrium, wave experiments are carried out. The time to reach equilibrium is typically in the order of 3–4 weeks. A typical equilibrium bubble radius a is of the order 10^{-2} m.

9. Reflection

A wave experiment proceeds as follows. A pressure difference is created over the membrane which separates the test section from the upper section (see figure 5). By means of an electric current, the membrane is ruptured, and a shock wave in air is generated, which is transmitted into the water layer on top of the porous test column. This wave then partially reflects and partially transmits into the test column. For a typical wave velocity in the porous test column of the order 10^3 m s^{-1}, the acoustic wavelength λ for a frequency of the order 10^4 Hz is of the order 10^{-1} m, which is an order of magnitude larger than the bubble radius. Hence direct acoustical variations of pressure and temperature within a bubble may be neglected. As $\lambda \gg a > \Lambda$, where

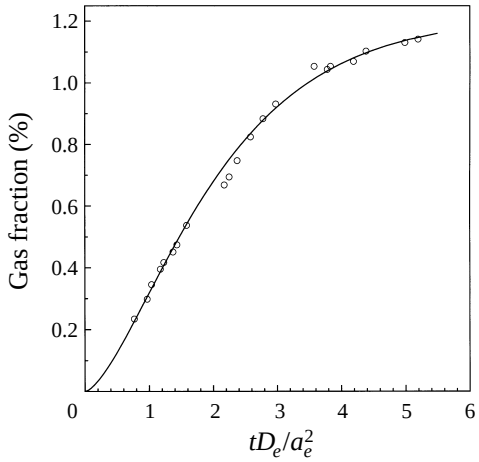

FIGURE 6. Gas bubble growth in time. The diffusion model is represented by the curve, which is fitted to the measurements by means of a least-squares method. The measurements are indicated by the circles.

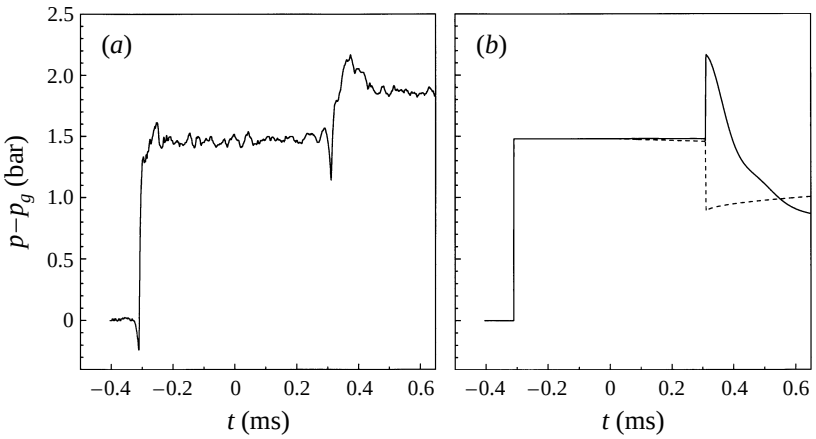

FIGURE 7. Experimental (*a*) and theoretical (*b*) reflection signals at $z = -46$ cm. Incident step-wise pressure wave: 1.48 bar. Gas volume fraction: 0.66%. Bubble radius: 2.9 mm. The dashed line refers to the quasi-stationary model. p_g is the atmospheric pressure.

Λ is the viscous length scale of the pores, a continuum approach may be used, and the Biot theory is fully applicable.

The recorded pressure at 46 cm above the column is shown in figure 7(*a*). The gas fraction in the column is 0.66 ± 0.01 % with a mean gas bubble radius of 2.9 ± 0.2 mm. We have reported reflection experiments previously, but so far only quasi-stationary models (van der Grinten *et al.* 1988) or approximate dynamic models (Sniekers *et al.* 1989) have been used. At $t = -0.31$ ms, the arrival of the incident wave is recorded. The initial negative pressure peak at that time is caused by the compliance of the shock tube. Because $t = 0$ is defined by the arrival of the incident wave at the top of the test column, the wave reflected from the column is recorded at $t = 0.31$ ms. The negative pressure peak is visible again, followed by a pressure overshoot and a subsequent gradual pressure decrease (see figure 7*a*). Our available measuring time is limited to approximately 0.7 ms, because the upgoing reflected wave will be reflected

from the free water surface, will propagate downward again and in this way act as a second incident wave.

In figure 7(*b*), theoretical pressure curves are presented for both the dynamic and quasi-stationary models. These theoretical curves are computed from the plane wave solutions (3.10) and (3.11). From the continuity of pressure and volume flux at the interface between the water layer and the porous test sample at $z = 0$, and using the condition that at the free surface of the test column the compressive stress vanishes, the amplitudes A_{s1} and A_{s2} in (3.10) and (3.11) can be calculated. Next, straightforward Fourier decomposition is used to compute the pressure–time plots in figure 7(*b*) (van der Grinten *et al.* 1985, 1987). It is obvious that the quasi-stationary model is unable to give an accurate description of the measurement. Instead of a pressure overshoot at $t = 0.31$ ms, a pressure decrease is predicted, followed by a gradual pressure increase. This negative reflection coefficient is caused by the high compressibility of the fluid.

In the dynamic model, the high-frequency limit of the fluid bulk modulus K_f is not affected by the gas bubbles (see figure 3). This results in a correct prediction of the height of the pressure overshoot at $t = 0.31$ ms. Also, the subsequent pressure decrease appears in our computations, but it is overestimated. This pressure decrease is caused by the high compressibility of the fluid for frequency components close to the gas bubble resonant frequency (see figure 3), resulting in negative reflection coefficients for those frequency components.

10. Transmission

In the same experiment, the pore pressures at 2 and 12 cm from the top of the column were also measured. Results are shown in figures 8(*a*) and 8(*c*), respectively. At 2 cm, a similar pressure behaviour as in the reflected signal is visible. A pressure overshoot is recorded, followed by a steep descent and a subsequent gradual pressure rise. Small oscillations are visible on the ascending slope of the pressure overshoot. In figure 8(*b*), the computed pressure signals are plotted for the dynamic model (solid line) and the quasi-stationary model (dashed line). Because of the high compressibility of the pore fluid, the first Biot wave hardly appears in the quasi-stationary model. This model only computes the second Biot wave, propagating at a speed of 74.5 m s^{-1}, and causing a diffusive pressure rise at $t = 0.27$ ms. Note that this velocity is lower than the speed of sound in air, which is caused by the fact that the gas bubbles substantially alter the compressibility of the pore fluid, but hardly influence its density.

From figures 8(*a*) and 8(*b*), we find that there is a good agreement between the measurements and the dynamic model. Because the pore fluid is relatively incompressible for high frequencies, the first Biot wave appears correctly in our computations, followed by the pressure decrease caused by the high compressibility of the pore fluid for frequencies close to the gas bubble resonant frequency. At 12 cm, we find that the first Biot wave has developed into an oscillatory pressure signal (see figure 8*c*). The oscillations are followed by a slow pressure rise. From the recordings at 2 and 12 cm, and from measurements involving the waves reflected from the bottom of the test sample, a wave speed of 2550 ± 180 m s^{-1} was determined. In figure 8(*d*), we have again plotted the computed dynamic and quasi-stationary pressures. Obviously, the quasi-stationary model (dashed line) does not predict any non-zero pressure readings until the arrival of the second Biot wave at $t = 1.61$ ms. It is therefore not visible on the time scale of figure 8(*d*).

Also in this case, we find that there is a good agreement between the experiment and

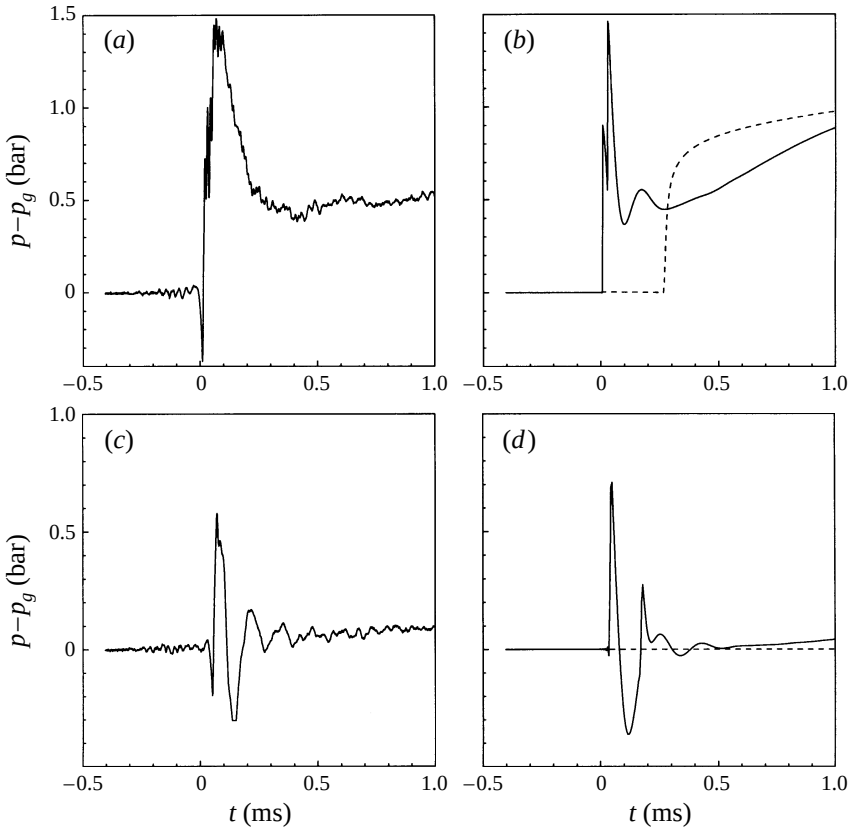

FIGURE 8. Experimental (a, c) and theoretical (b, d) pore pressure signals at $z = 2$ (a, b) and $z = 12$ (c, d) cm. Incident step-wise pressure wave: 1.48 bar. Gas volume fraction: 0.66 %. Bubble radius: 2.9 mm. The dashed lines refer to the quasi-stationary model. p_g is the atmospheric pressure.

the dynamic model (see figures 8*c* and 8*d*). The oscillations are predicted correctly and so is the subsequent slow pressure rise. The theoretical wave velocity is 2866 m s^{-1}, which is equal to the theoretical velocity of the fastest wave in the high-frequency limit (see figure 4). This velocity is slightly higher than the measured wave velocity, which may be caused by the fact that the experimental configuration cannot fully be described by a one-dimensional model. Also, the stiffness of the matrix, determined by the dry constrained modulus K_p, may have decreased upon contact with the water. A further comparison between experiment and theory is made in figure 9, where the frequency spectra of the oscillations are shown. It appears that there is a distinct frequency maximum in the measurement at $\omega = (4.9 \pm 0.2) \times 10^4$ s^{-1}. The theoretical frequency maximum is somewhat lower (3.2×10^4 s^{-1}), but there is a good overall agreement between experiment and theory. It is found that the frequency maximum in the pressure signal corresponds to an anti-resonance type of bubble oscillation as described in § 7. The frequency of this oscillation is significantly higher than the resonant frequency of the gas bubbles ($\omega_r = 2099$ s^{-1}).

At the same depth of 12 cm, the influence of a change in gas bubble size and concentration is investigated. New measurements were performed for a smaller gas bubble size and concentration: $(1-s) = 0.12 \pm 0.01\%$ and $a = 0.6 \pm 0.2$ mm. The result is plotted in figure 10(*a*). Also in this case an oscillatory pore pressure behaviour is

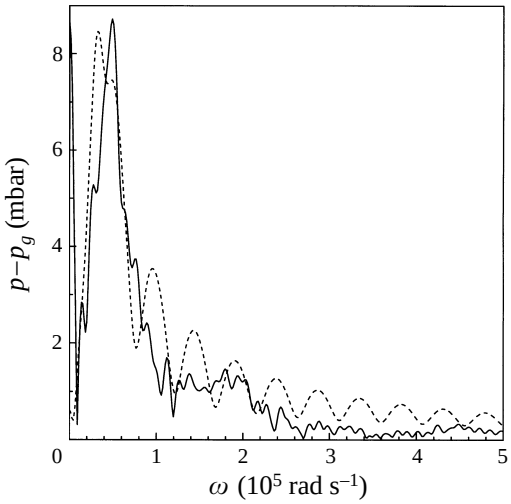

FIGURE 9. Amplitude spectra of the recorded (solid line) and computed (dashed line) pore pressure signals at $z = 12$ cm. Incident step-wise pressure wave: 1.48 bar. Gas volume fraction: 0.66%. Bubble radius: 2.9 mm. p_g is the atmospheric pressure.

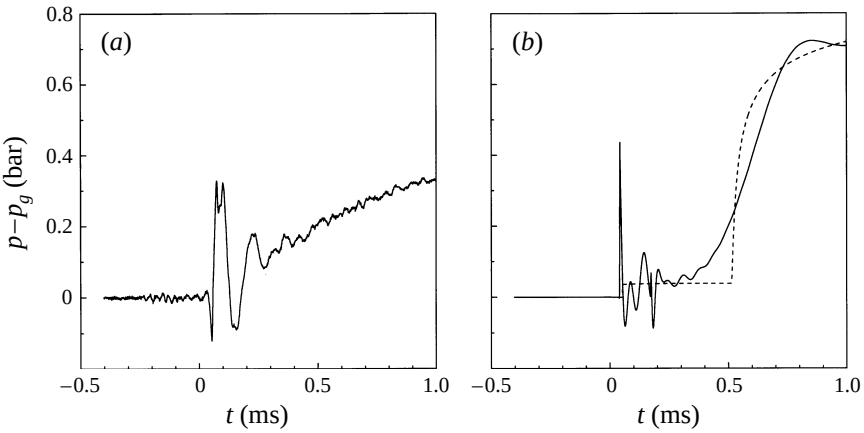

FIGURE 10. Experimental (*a*) and theoretical (*b*) pore pressure signals at $z = 12$ cm. Incident step-wise pressure wave: 0.82 bar. Gas volume fraction: 0.12%. Bubble radius: 0.6 mm. The dashed line refers to the quasi-stationary model. $p_g = 2$ bar.

recorded. The subsequent pressure rise, however, is much stronger than in figure 8(*c*). The oscillatory wave propagates with a velocity of 2560 ± 190 m s^{-1}. This velocity is the same as in the less saturated case, which means that this wave velocity is hardly influenced by the size and concentration of the gas bubbles. Corresponding theoretical curves for the dynamic and quasi-stationary model are given in figure 10(*b*). Contrary to figure 8(*d*), the first Biot wave is visible in the quasi-stationary computation (dashed line). It appears as a small step wave at $t = 0.05$ ms, propagating with a velocity of 2269 m s^{-1}, which is lower than the measured velocity of the oscillating wave. The second Biot wave, propagating with a velocity of 234.7 m s^{-1} is visible as a diffusive pressure rise at $t = 0.51$ ms. No oscillations are computed.

From figures 10(*a*) and 10(*b*), we find that all essential aspects of the measurement are predicted by the dynamic model. An oscillating wave is computed, propagating

with a velocity of 2863 m s^{-1}. As before, the measured velocity is slightly lower than this computed value. Also, the strong pressure rise is visible in our dynamic computations, but it appears overestimated. From figures 10(*a*) and 10(*b*), it is clear that the measured frequencies of the oscillations are lower than predicted. This is probably caused by inhomogeneities in the gas bubble distribution.

11. Conclusions

We have developed a dynamic model for the compressibility of pore fluid containing small gas bubbles. In this model viscous and thermal damping of oscillating gas bubbles are taken into account. A Biot damping mechanism is introduced, consisting of Darcy and compressibility effects. It appears that the Darcy damping is the dominant mechanism, but compressibility effects become equally important for high frequencies. An interesting aspect of this model is that the high-frequency compressibility of the pore fluid is virtually not affected by the presence of the gas bubbles and is almost the same as in the fully saturated case. In this respect, the dynamic model is different from the quasi-stationary model, in which the influence of a small gas fraction in the pores on the fluid compressibility is predominant and identical for all frequencies. This dynamic fluid model was incorporated in the Biot theory for plane wave propagation in poro-elastic media. It was found that small gas saturations have very important effects on wave velocities and damping coefficients. Strong pore pressure oscillations were predicted, propagating in the porous medium with relatively high velocities and low damping coefficients.

These effects were experimentally investigated in a shock tube. Using a supersaturation technique, a homogeneous gas–liquid mixture in a porous test sample was obtained. Gas bubble size and concentration were independently measured by means of compressibility measurements. All relevant physical properties of the test sample were also determined independently. For the pore pressures, an oscillating wave mode was recorded indeed, whose velocity was not influenced by the size and concentration of the gas bubbles, but mainly by the physical properties of the porous structure. As predicted by our modified Biot model for plane wave propagation, the frequencies of this wave mode were found to correspond to an anti-resonance type of gas bubble oscillation, with frequencies higher than the bubble resonant frequency. These frequencies are determined by the size and concentration of the gas bubbles in the pores.

For the reflected waves, an initial pressure overshoot was recorded, followed by a pressure decrease. This initial overshoot is caused by the low compressibility of the pore fluid for high frequencies, whereas the pressure decrease is caused by the high compressibility of the pore fluid for frequencies close to the gas bubble resonant frequency.

We would like to thank A. A. M. Wasser for constructing the experimental set-up and the anonymous referees for their suggestions. This work was supported by Grant No. ETN 37.1274 of the Netherlands Foundation for Fundamental Research on Matter.

Appendix. Gas bubble growth

Following Smeulders *et al.* (1992*a*), a quasi-steady description of the diffusion-dominated bubble growth process is given. Considering a gas bubble of radius $a(t)$,

we define the origin of coordinates at the bubble centre, which is at rest. The position of any point in the fluid is indicated by its distance r from the origin. A stepwise ambient pressure decrease will cause the fluid to be super-saturated, and gas bubble growth begins. A reduced dissolved gas density C at a fixed time t may be defined:

$$C = \frac{\rho_d(r,t) - \rho_{d\infty}(t)}{\rho_{da} - \rho_{d\infty}(t)}, \tag{A 1}$$

where ρ_d is the dissolved gas density in the fluid, ρ_{da} is the dissolved gas density at $r = a$, and $\rho_{d\infty}$ is the dissolved gas density far away from the bubble. From the quasi-steady diffusion equation $\nabla^2 C = 0$, we find that $C(t) = a(t)/r$. The mass flux from the fluid towards the gas bubble may now be calculated:

$$\tfrac{4}{3}\pi\rho_g \frac{\mathrm{d}a^3(t)}{\mathrm{d}t} = -4\pi a(t) D_e \left[\rho_{da} - \rho_{d\infty}(t)\right], \tag{A 2}$$

where D_e is an effective diffusion constant. It is equal to the diffusion constant D in water, modified by the tortuosity parameter α_∞: $D_e = D/\alpha_\infty$ (Smeulders *et al.* 1992*a*). For a large number of bubbles with number density N m^{-3}, we define the average distance between bubbles $2a_e$ as $N^{-1/3}$. If this average distance far exceeds the bubble radius, equation (A 2) still holds if we replace the factor $\rho_{d\infty}(t)$ by the dissolved gas density $\rho_{de}(t)$ at $r = a_e$. For the mass conservation law we may write

$$\tfrac{4}{3}\pi\rho_g a^3(t) + \int_{a(t)}^{a_e} 4\pi r^2 \rho_d(r,t)\mathrm{d}r = \tfrac{4}{3}\pi\rho_{d0} a_e^3, \tag{A 3}$$

where ρ_g is the uniform gas density in the bubble, and ρ_{d0} is the uniform dissolved gas density at $t = 0$. To a good approximation, the integral in (A 3) is equal to $\frac{4}{3}\pi\rho_{de}(t)\left[a_e^3 - a^3(t)\right]$. Assuming $a^3(t) \ll a_e^3$, we find from equation (A 3)

$$\rho_{de}(t) = \rho_{d0} - \rho_g \frac{a^3(t)}{a_e^3}. \tag{A 4}$$

Substitution of this equation in (A 2) yields a differential equation for the reduced bubble radius $\eta(t) = a(t)/a_e$:

$$\eta \frac{\mathrm{d}\eta}{\mathrm{d}t'} = \eta_\infty^3 - \eta^3, \tag{A 5}$$

where $\eta_\infty^3 = (\rho_{d0} - \rho_{da})/\rho_g$. Furthermore, we have introduced the reduced time $t' = D_e t/a_e^2$. When the diffusion process is approaching its new equilibrium state for $t' \to \infty$, obviously $\mathrm{d}\eta/\mathrm{d}t'$ will tend to zero and $\eta \to \eta_\infty$. Solving the differential equation (A 5), we find

$$t' = \frac{1}{6\eta_\infty} \ln \frac{\eta_\infty^2 + \eta_\infty\eta + \eta^2}{(\eta_\infty - \eta)^2} + \frac{1}{\eta_\infty\sqrt{3}} \left[\frac{\pi}{6} - \arctan \frac{2\eta + \eta_\infty}{\eta_\infty\sqrt{3}}\right]. \tag{A 6}$$

The relation between the bubble radius and the gas fraction is given by

$$\frac{a^3(t)}{a_e^3} = \eta^3(t) = 1 - s(t). \tag{A 7}$$

REFERENCES

Achenbach, J. D. 1973 *Wave Propagation in Elastic Solids*. North-Holland.

Allard, J.-F. 1993 *Propagation of Sound in Porous Media*. Elsevier.

Anderson, A. L. & Hampton, L. D. 1980*a* Acoustics of gas-bearing sediments I. Background. *J. Acoust. Soc. Am.* **67**, 1865–1889.

Anderson, A. L. & Hampton, L. D. 1980*b* Acoustics of gas-bearing sediments II. Measurements and models. *J. Acoust. Soc. Am.* **67**, 1890–1903.

Auriault, J. L. 1980 Dynamic behaviour of a porous medium saturated by a Newtonian fluid. *Intl J. Engng Sci.* **18**, 775–785.

Auriault, J. L., Borne, L. & Chambon, R. 1985 Dynamics of porous saturated media, checking of the generalized low of Darcy. *J. Acoust. Soc. Am.* **77**, 1641–1650.

Bear, J. & Bachmat, Y. 1990 *Introduction to Modeling of Transport Phenomena in Porous Media*. Kluwer.

Bedford, A. & Stern, M. 1983 A model for wave propagation in gassy sediments. *J. Acoust. Soc. Am.* **73**, 409–417.

Berryman, J. G., Thigpen, L. & Chin, R. C. Y. 1988 Bulk elastic wave propagation in partially saturated porous solids. *J. Acoust. Soc. Am.* **84**, 360–373.

Biot, M. A. 1956*a* Theory of propagation of elastic waves in a fluid-saturated solid. I. Low frequency range. *J. Acoust. Soc. Am.* **28**, 168–178.

Biot, M. A. 1956*b* Theory of propagation of elastic waves in a fluid-saturated solid. II. Higher frequency range. *J. Acoust. Soc. Am.* **28**, 179–191.

Bird, R. B., Stewart, W. E. & Lightfoot, E. N. 1960 *Transport Phenomena*. John Wiley and Sons.

Champoux, Y. & Allard, J.-F. 1991 Dynamic tortuosity and bulk modulus in air-saturated porous media. *J. Appl. Phys.* **70**, 1975–1979.

Devin, C. 1959 Survey of thermal, radiation and viscous damping of pulsating air bubbles in water. *J. Acoust. Soc. Am.* **31**, 1654–1667.

Dontsov, V. E., Kuznetsov, V. V. & Nakoryakov, V. E. 1987 Pressure waves in a porous medium saturated with a gassy fluid. *Mekh. Zhidk. i Gaza* **4**, 85–92.

Foldy, L. L. 1945 The multiple scattering of waves. *Phys. Rev.* **67**, 107–119.

Garg, S. K. & Nayfeh, A. H. 1986 Compressional waves propagation in liquid-saturated elastic porous media. *J. Appl. Phys.* **60**, 3045–3055.

Geertsema, T. & Smit, D. C. 1961 Some aspects of elastic wave propagation in fluid-saturated porous solids. *Geophysics* **26**, 169–181.

Grinten, J. G. van der, Dongen, M. E. H. van & Kogel, H. van der 1985 A shock tube technique for studying pore pressure propagation in a dry and water-saturated porous medium. *J. Appl. Phys.* **58**, 2937–2942.

Grinten, J. G. van der, Dongen, M. E. H. van & Kogel, H. van der 1987 Strain and pore pressure propagation in a water-saturated porous medium. *J. Appl. Phys.* **62**, 4682–4687.

Grinten, J. G. van der, Sniekers, R. W. J. M., Dongen, M. E. H. van & Kogel, H. van der 1988 An experimental study of shock-induced wave propagation in dry, water-saturated, and partially saturated porous media. In *Proc. Intl Symp. on Modelling Soil-Water-Structure Interactions* (ed. P. A. Kolkman, J. Lindenberg & K. W. Pilarczyk), pp. 469–478. Balkema.

Henry, M., Lemarinier, P., Allard, J.-F., Bonardet, J. L. & Gedeon, A. 1995 Evaluation of the characteristic dimensions for porous sound-absorbing materials. *J. Appl. Phys.* **77**, 17–20.

Johnson, D. L., Koplik, J. & Dashen, R. 1987 Theory of dynamic permeability and tortuosity in fluid-saturated porous media. *J. Fluid Mech.* **176**, 379–402.

Johnson, D. L. & Plona, T. J. 1982 Acoustic slow waves and the consolidation transition. *J. Acoust. Soc. Am.* **72**, 556–565.

Lévy, T. 1979 Propagation of waves in a fluid-saturated porous elastic solid. *Intl J. Engng Sci.* **17**, 1005–1014.

Pfriem, H. 1940 Zur thermischen Dämpfung in kugelsymmetrisch schwingende Gasblasen. *Akust. Z.* **5**, 202.

Plesset, M. S. 1949 The dynamics of cavitation bubbles. *J. Appl. Mech.* **16**, 277–282.

Prosperetti, A. 1984 Bubble phenomena in sound fields: part one. *Ultrasonics* **22**, 69–77.

Prosperetti, A. 1991 The thermal behaviour of oscillating gas bubbles. *J. Fluid Mech.* **222**, 587–616.

Sangani, A. S. 1991 A pairwise interaction theory for determining the linear acoustic properties of dilute bubbly liquids. *J. Fluid Mech.* **232**, 221–284.

Sangani, A. S. & Sureshkumar, R. 1993 Linear acoustic properties of bubbly liquids near the natural frequency of the bubbles using numerical simulations. *J. Fluid Mech.* **252**, 239–264.

Smeulders, D. M. J., De la Rosette, J. P. M. & Dongen, M. E. H. van 1992*a* Waves in partially saturated porous media. *Transport in Porous Media.* **9**, 25–37.

Smeulders, D. M. J., Eggels, R. L. G. M. & Dongen, M. E. H. van 1992*b* Dynamic permeability: reformulation of theory and new experimental and numerical data. *J. Fluid Mech.* **245**, 211–227.

Smeulders, D. M. J., Van Hassel, R. R., Dongen, M. E. H. van & Jansen, J. K. M. 1994 Similarity of sharp–edged porous media. *Intl J. Engng Sci.* **32**, 979–990.

Sniekers, R. W. J. M., Smeulders, D. M. J., Dongen, M. E. H. van & Kogel, H. van der 1989 Pressure wave propagation in a partially water-saturated porous medium. *J. Appl. Phys.* **66**, 4522–4524.

Spitzer, L. 1943 Acoustical properties of gas bubbles in a liquid. *NRDC Rep.* 6, 1-sr20-918, PB31026. Columbia University Office of Scientific Research and Development.

Stoll, R. D. 1974 Acoustic waves in saturated sediments. In *Physics of Sound in Marine Sediments* (ed. L. D. Hampton). Plenum.

Stralen, S. van & Cole, R. 1979 *Boiling Phenomena.* Hemisphere.

Verruijt, A. 1982 The theory of consolidation. In *Proc. NATO Advanced Study Institute on Mechanics of Fluids in porous media*, pp. 349–368. Nijhoff.

Ward, C. A., Johnson, W. R., Venter, R. D., Ho, S., Forest, T. W. & Fraser, W. D. 1983 Heterogeneous bubble nucleation and conditions for growth in a liquid-gas system of constant mass and volume. *J. Appl. Phys.* **54**, 1833–1843.

Wijngaarden, L. van 1970 On the structure of shock waves in liquid-bubble mixtures. *Appl. Sci. Res.* **22**, 366–381.

Wijngaarden, L. van 1972 One dimensional flow of liquids containing small gas bubbles. *Ann. Rev. Fluid Mech.* **4**, 369–395.

Wood, A.B. 1955 *A Textbook of Sound.* Bell.